



Cite this: *CrystEngComm*, 2015, 17, 3312

Mixed-metal–organic frameworks (M'MOFs) from 1D to 3D based on the “organic” connectivity and the inorganic connectivity: syntheses, structures and magnetic properties†

Sheng Zhang,^a Xiangyu Liu,^{ab} Qi Yang,^a Qing Wei,^a Gang Xie^a and Sanping Chen^{*a}

Based on the I^nO^m notion (I^n = the dimensionality of the inorganic connectivity; O^m = the dimensionality of the organic connectivity; $n + m \leq 3$), we obtained ten transition/alkaline earth mixed-metal–organic frameworks (M'MOFs) from 1D to 3D through a “metalloligand” strategy at room temperature. Single-crystal X-ray diffraction analyses indicate that the resulting compounds possess the square plane $[M^{II}-(pzdc)_2]^{2-}$ (M = Co, Ni or Cu) “organic” connectivity and the Ae–O–Ae (Ae = Ca, Sr or Ba) inorganic connectivity, which can be classified as I^1O^0 connectivity for complexes 1, 4, 7 and 9, I^1O^1 connectivity for complexes 2, 3, 5, 6 and 8 and I^1O^2 connectivity for complex 10. The $[M^{II}-(pzdc)_2]^{2-}$ moieties acting as bis(tetridentate) polycarboxylate ligands show three types of coordination modes, namely μ_4 -(η^2 -O,O)₂(η^1 -O')₂, μ_6 -(η^2 -O,O)₂(η^1 -O')₂ and μ_{10} -(η^2 -O,O)₂(η^2 -O',O')₂, (η^1 -O')₂(η^1 -O')₂(η^1 -N')₂. Additionally, the thermal stabilities of complexes 1–10 and magnetic properties of complexes 1, 2, 4, 5 and 10 have also been investigated.

Received 20th January 2015,
Accepted 11th March 2015

DOI: 10.1039/c5ce00126a

www.rsc.org/crystengcomm

Introduction

The chemistry of mixed-metal–organic frameworks (M'MOFs) containing both transition metals and alkaline earth metals (Ae) has attracted widespread attention due to their pleasing architectures and potential applications for catalysis, materials science and biochemistry.^{1–5} There still exist formidable challenges for the predesigned and directional syntheses of M'MOFs because (1) alkaline earth metal ions with large radii and high coordination numbers make the topologies of coordination polymers uncontrollable; (2) according to the hard–soft acid–base theory, transition metal ions and alkaline earth metal ions have different affinities for N- and O-donors, frequently resulting in homometallic complexes.⁵

As known, N-heterocyclic polycarboxylates with O- and N-donors, such as 3,5-pyrazoledicarboxylic acid (H₃pdC) and

pyridine-2,3-dicarboxylic acid (2,3-H₂pydc), are usually employed to construct mixed-metal polymers in one-pot synthesis.^{4,5} In general, the ligand tends to chelate one metal with O- and N-donors from the carboxyl group and pyridine ring, leaving unsaturated O-donors to bind other metals. However, the reaction conditions, such as the reaction temperature, pH value of the system and reagent ratio, need to be regulated and controlled precisely. Accordingly, a step-by-step and controllable method would be better than one-pot synthesis in a “black box”. Realistically speaking, we can synthesize stable “organic” fragments containing transition metals and unsaturated carboxylic oxygen atoms first and then make these fragments react with other metals. For example, Pardo *et al.* used a Cu^{II} precursor as a bis(bidentate) ligand (metalloligand) to bind to other transition cations to afford a family of M^{II}/Cu^{II} (M = Mn, Co) heterobimetallic single-chain magnets (SCMs).⁶ To summarize, the stepwise “metalloligand” strategy for the construction of mixed-metal polymers begins with the following recognitions:^{6–8} (1) the organic ligand possesses at least two possible coordination sites, which can be used to synthesize a relatively stable precursor; (2) the precursor with potential coordination donors could link other metal ions.

Additionally, arrays of inorganic connectivities, M–X–M (M = metals, X = O, Cl, N, or S) in extended inorganic hybrids have peculiar magnetic, electronic and optical properties.^{9,10} Polycarboxylate ligands with organic connectivity have been

^a Key Laboratory of Synthetic and Natural Functional Molecule Chemistry of Ministry of Education, College of Chemistry and Materials Science, Northwest University, Xi'an 710127, China. E-mail: sanpingchen@126.com

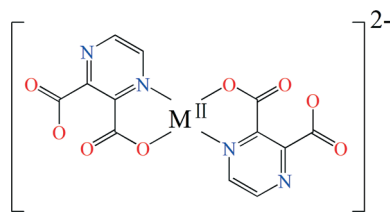
^b School of Chemistry and Chemical Engineering, Ningxia University, Yinchuan 750021, China

† Electronic supplementary information (ESI) available: X-ray crystallographic files in CIF format have been deposited with the Cambridge Structural Database as files. CCDC 853803, 853809, 853811, 1039841, 1039842, 853894, 1039839, 853810, 1039840 and 1039838 for crystals 1–10 contain the supplementary crystallographic data for this paper. For ESI and crystallographic data in CIF or other electronic format see DOI: 10.1039/c5ce00126a

widely used to construct various MOFs with intriguing properties.¹¹ Alkaline earth metal ions of relatively larger radius and high affinity for oxygen donors exhibit unparalleled opportunities to construct extended inorganic–organic hybrids with rigid aromatic polycarboxylate ligands. Coincidentally, Yao *et al.* reported a series of Ca(II) or Ba(II) inorganic–organic hybrid frameworks from 1D to 3D constructed by aromatic polycarboxylate ligands and the M–O–M (M = Ca, Ba) inorganic connectivity, which could be classified as I¹O¹, I²O⁰ and I³O⁰ structures (Iⁿ = the dimensionality of the inorganic connectivity; O^m = the dimensionality of the organic connectivity; n + m ≤ 3).¹² The connectivity of the extended hybrid framework can be described using the IⁿO^m notion.

Beyond all doubt, based on the IⁿO^m notion above, it is worth trying to combine the characteristics of a “metalloligand” with unsaturated O-donors and alkaline earth metal ions inclining to coordinate with oxygen atoms (M–O–M). Herein, [Cu^{II}(pzdc)₂]²⁻/[M^{II}(Hpzdc)₂] (ref. 13) (M = Co or Ni; 2,3-H₂Hpzdc = pyrazine-2,3-dicarboxylic acid¹⁴) are selected as bis(tetradeятate) ligands (metalloligands) to bind to the alkaline earth cations to construct M'MOFs based on the following reasons: (1) a symmetrically stable square plane only including a monometal ion (Scheme 1), [M^{II}(pzdc)₂]²⁻ (M = Co, Ni or Cu), exists in a large number of reported complexes based on statistical data of CCDC (crystallographic database, about 53.8% possessing [Cu^{II}(pzdc)₂]²⁻ species in reported Cu-complexes, 75.0% possessing [Ni^{II}(pzdc)₂]²⁻ species in reported Ni-complexes and 53.3% possessing [Co^{II}(pzdc)₂]²⁻ species in reported Co-complexes, see the ESI†); (2) the precursor with O-donors acting as “the rigid aromatic polycarboxylate ligand” (O^m) could link the inorganic connectivity (Iⁿ), Ae–O–Ae (Ae = Ca, Sr or Ba), obtaining extended hybrid frameworks.

Employing the strategy above, we obtained a series of new transition/alkaline earth heterometallic MOFs by reaction of “metalloligands” [Cu^{II}(pzdc)₂]²⁻/[M^{II}(Hpzdc)₂] (M = Co or Ni) with different alkaline earth metal salts, described as [Ca₂Co(pzdc)₂(NO₃)₂(H₂O)₈]_n·2nH₂O (**1**), [Sr₂Co(pzdc)₂(H₂O)₁₀]_n·2nCl (**2**), [Ba₂Co(pzdc)₂(H₂O)₁₀]_n·2nCl (**3**), [Ca₂Ni(pzdc)₂(NO₃)₂(H₂O)₈]_n·2nH₂O (**4**), [Sr₂Ni(pzdc)₂(H₂O)₁₀]_n·2nCl (**5**), [Ba₂Ni(pzdc)₂(H₂O)₁₀]_n·2nCl (**6**), [Ca₂Cu(pzdc)₂(NO₃)₂(H₂O)₈]_n (**7**), [Sr₂Cu(pzdc)₂(Cl)₂(H₂O)₁₀]_n (**8**), [Sr₂Cu(pzdc)₂(NO₃)₂(H₂O)₁₀]_n (**9**) and [Ba₂Cu(pzdc)₂Cl(H₂O)₃]_n (**10**). All structures are built by square plane units [M^{II}(pzdc)₂]²⁻ (M = Co, Ni or Cu) and the Ae–O–Ae (Ae = Ca, Sr or Ba) inorganic connectivity. Additionally, the thermal stabilities of complexes **1**–**10** and



Scheme 1 The square plane containing metal(II) cations, [M^{II}(pzdc)₂]²⁻ (M = Co, Ni or Cu).

magnetic properties of complexes **1**, **2**, **4**, **5** and **10** have also been investigated.

Experimental section

Materials and chemicals

All other chemicals were used from commercial sources without further purification. Elemental analyses (C, H and N) were performed using an Elementar Vario EL III elemental analyzer. Infrared spectra were obtained from KBr pellets using a Bruker EQUINOX 55 Fourier transform infrared spectrometer in the range 400–4000 cm⁻¹. Thermogravimetric analyses (TGA) were performed using a PerkinElmer Pyris Diamond TG-DTA between 30 and 900 °C in oxygen-free nitrogen atmosphere with a heating rate of 10 °C min⁻¹ with α-Al₂O₃ as a standard material. Magnetic measurements were accomplished on polycrystalline samples (13.32 mg of **1**, 13.76 mg of **2**, 11.39 mg of **4**, 15.01 mg of **5** and 12.33 mg of **10**) using a Quantum Design MPMS-XL7 SQUID magnetometer at temperatures between 2 and 300 K for direct current (dc) applied fields with an applied field of 1 kOe (restrained in eicosane to prevent torquing at high fields). The measured susceptibilities were corrected for the diamagnetism of the constituent atoms (Pascal's tables). Variable-field (0–5 T) magnetization measurements at 2.0 K were carried out using a Quantum Design SQUID magnetometer.

Synthesis of “metalloligands”

[Co(Hpzdc)₂(H₂O)₂] (*L*_{Co}),^{13a} [Ni(Hpzdc)₂(H₂O)₂] (*L*_{Ni})^{13b} and [Cu(pzdc)₂(H₂O)₂]·2ampy·6H₂O (*L*_{Cu})^{13c} (H₂Pzdc = pyrazine 2,3-dicarboxylic acid, ampy = 2-amino-4-methylpyridine) were synthesized according to references.

Synthesis of [Ca₂Co(pzdc)₂(NO₃)₂(H₂O)₈]_n·2nH₂O (**1**). *L*_{Co} (0.43 g, 1 mmol) was dissolved in 20 mL of ethanol. Ca(NO₃)₂·4H₂O (0.48 g, 2 mmol) was then added to the mixture with stirring at room temperature for half an hour. The filtrate was allowed to evaporate slowly at room temperature. After several days, orange rod crystals were obtained in 31% yield based on Ca(II) ions. Anal. calcd for C₁₂H₂₄Ca₂CoN₆O₂₄ (775.46): C 18.57%, H 3.09%, N 10.83%; found: C 18.69%, H 3.22%, N, 10.79%. IR data (KBr pellet, cm⁻¹): 3522(s), 3245(w), 1611(s), 1571(s), 1459(s), 1433(s), 1389(s), 1368(s), 1277(m), 1233(m), 1169(w), 1150(m), 1110(w), 1056(w), 988(w), 944(w), 877(w), 849(s), 833 (s), 821(m), 767 (w), 710(s), 700(s), 654(s).

Synthesis of [Sr₂Co(pzdc)₂(H₂O)₁₀]_n·2nCl (**2**). The synthetic procedure for **2** is similar to that for **1** except Ca(NO₃)₂·4H₂O was replaced with SrCl₂·6H₂O (0.54 g, 2 mmol). Yield: 26%, based on Sr(II) ions. Anal. calcd for C₁₂H₂₄Cl₂CoN₄O₁₈Sr₂ (817.42): C 17.62%, H 2.94%, N 6.85%; found: C 17.51%, H 2.88%, N 6.75%. IR data (KBr pellet, cm⁻¹): 3455 (s), 3032 (w), 1622(s), 1549(s), 1443(s), 1409(s), 1366(s), 1099(s), 860(s), 782(s), 751(s), 706(s), 655(s), 631(w).

Synthesis of [Ba₂Co(pzdc)₂(H₂O)₁₀]_n·2nCl (**3**). The synthetic procedure for **3** is similar to that for **1** except Ca(NO₃)₂·4H₂O was replaced with BaCl₂ (0.41 g, 2 mmol). Yield: 22% based

on Ba(II) ions. Anal. calcd for $C_{12}H_{24}Ba_2CoN_4O_{18}Cl_2$ (916.86): C 15.71%, H 2.62%, N 6.11%; found: C 15.81%, H 2.50%, N 6.28%. IR data (KBr pellet, cm^{-1}): 3480(s), 3076(w), 1613(s), 1573(s), 1452(s), 1410(s), 1379(s), 1101(s), 848(s), 771(s), 722(s), 704(s), 692(s), 601(w).

Synthesis of $[Ca_2Ni(pzdc)_2(NO_3)_2(H_2O)_8]_n \cdot 2nH_2O$ (4). The synthetic procedure for 4 is similar to that for 1 except L_{Co} was replaced with L_{Ni} (0.43 g, 1 mmol). Yield: 33% based on Ca(II) ions. Anal. Calcd for $C_{12}H_{24}Ca_2NiN_6O_{24}$ (775.24): C 18.57%, H 3.10%, N 10.84%; found: C 18.69%, H, 3.33%, N 10.69%. IR data (KBr pellet, cm^{-1}): 3521(s), 3244(w), 1619(s), 1558(s), 1459(s), 1443(s), 1400(s), 1370(s), 1262(m), 1244 (m), 1170(w), 1133(m), 1115(w), 1049(w), 980(w), 950(w), 877(w), 846(s), 840(s), 821(m), 776(w), 711(s), 702(s), 670(s), 660(w).

Synthesis of $[Sr_2Ni(pzdc)_2(H_2O)_{10}]_n \cdot 2nCl$ (5). The synthetic procedure for 5 is similar to that for 2 except L_{Co} was replaced with L_{Ni} (0.43 g, 1 mmol). Yield: 23.2% based on Sr(II) ions. Anal. calcd for $C_{12}H_{24}Sr_2NiN_4O_{18}Cl_2$ (817.20): C 17.62%, H 2.94%, N 6.85%; found: C, 17.80%, H 3.11%, N 7.13%. IR data (KBr pellet, cm^{-1}): 3467(s), 3059(w), 1610(s), 1582(s), 1456(s), 1405(s), 1370(s), 1106 (s), 847(s), 788 (s), 742(s), 705(s), 669(s), 621(w).

Synthesis of $[Ba_2Ni(pzdc)_2(H_2O)_{10}]_n \cdot 2nCl$ (6). The synthetic procedure for 6 is similar to that for 3 except L_{Co} was replaced with L_{Ni} (0.43 g, 1 mmol). Yield: 41% based on Ba(II) ions. Anal. calcd for $C_{12}H_{24}Ba_2NiN_4O_{18}Cl_2$ (916.64): C 15.71%, H 2.62%, N 6.11%; found: C 15.86%, H, 2.81%, N 6.29%. IR data (KBr pellet, cm^{-1}): 3482(s), 3060(w), 1610(s), 1566(s), 1455(s), 1421(s), 1379(s), 1119(s), 851(s), 789(s), 740(s), 713(s), 680(s), 600(w).

Synthesis of $[Ca_2Cu(pzdc)_2(NO_3)_2(H_2O)_8]_n$ (7). The synthetic procedure for 7 is similar to that for 1 except L_{Co} was replaced with L_{Cu} (0.26 g, 1 mmol). Yield: 55% based on Ca(II) ions. Anal. calcd for $C_{12}H_{20}Ca_2CuN_6O_{22}$ (744.04): C 19.35%, H 2.69%, N 11.29%; found: C 19.41%, H, 2.82%, N 11.48%. IR data (KBr pellet, cm^{-1}): 3522(s), 3249(w), 1631(s), 1555(s), 1470(s), 1456(s), 1410(s), 1390(s), 1277(m), 1240(m), 1180(w), 1151(m), 1111(w), 1049 (w), 986(w), 949(w), 891(w), 861(s), 841(s), 822(m), 787(w), 720(s), 693(s), 659(s), 660(w).

Synthesis of $[Sr_2Cu(pzdc)_2(Cl)_2(H_2O)_{10}]_n$ (8). The synthetic procedure for 7 is similar to that for 2 except L_{Co} was replaced with L_{Cu} (0.26 g, 1 mmol). Yield: 61% based on Sr(II) ions. Anal. calcd for $C_{12}H_{24}Sr_2CuN_4O_{18}Cl_2$ (822.03): C 17.52%, H 2.92%, N 6.81%; found: C 17.88%, H 3.16% N, 7.01%. IR data (KBr pellet, cm^{-1}): 3444(m), 1623(s), 1580(s), 1380(s), 1120(s), 879(s), 844(s), 735(s), 704(s), 622(s), 469(s).

Synthesis of $[Sr_2Cu(pzdc)_2(NO_3)_2(H_2O)_{10}]_n$ (9). The synthetic procedure for 9 is similar to that for 7 except $Ca(NO_3)_2 \cdot 4H_2O$ was replaced with $Sr(NO_3)_2$ (0.42 g, 2 mmol). Yield: 46% based on Sr(II) ions. Anal. calcd for $C_{12}H_{24}Sr_2CuN_6O_{24}$ (875.15): C 16.45%, H 2.74%, N 9.60%; found: C 16.79%, H 2.51%, N 9.48%. IR data (KBr pellet, cm^{-1}): 3470(s), 3066(w), 1610(s), 1590(s), 1458(s), 1422(s), 1370(s), 1119(s), 840(s), 771(s), 745(s), 723(s), 670(s), 611(w).

Synthesis of $[Ba_2Cu(pzdc)_2Cl(H_2O)_3]_n$ (10). The synthetic procedure for 10 is similar to that for 3 except L_{Co} was

replaced with L_{Cu} (0.26 g, 1 mmol). Yield: 46% based on Ba(II) ions. Anal. calcd for $C_{12}H_{10}Ba_2CuN_4O_{11}Cl$ (759.91): C 18.95%, H 1.32%, N 7.37%; found: C 19.13%, H 1.51%, N 7.43%. IR data (KBr pellet, cm^{-1}): 3470(s), 3066(w), 1611(s), 1559(s), 1449(s), 1420(s), 1377(s), 1112(s), 850(s), 769(s), 731(s), 711(s), 688(s), 612(w).

Single-crystal X-ray data collection and structure determination

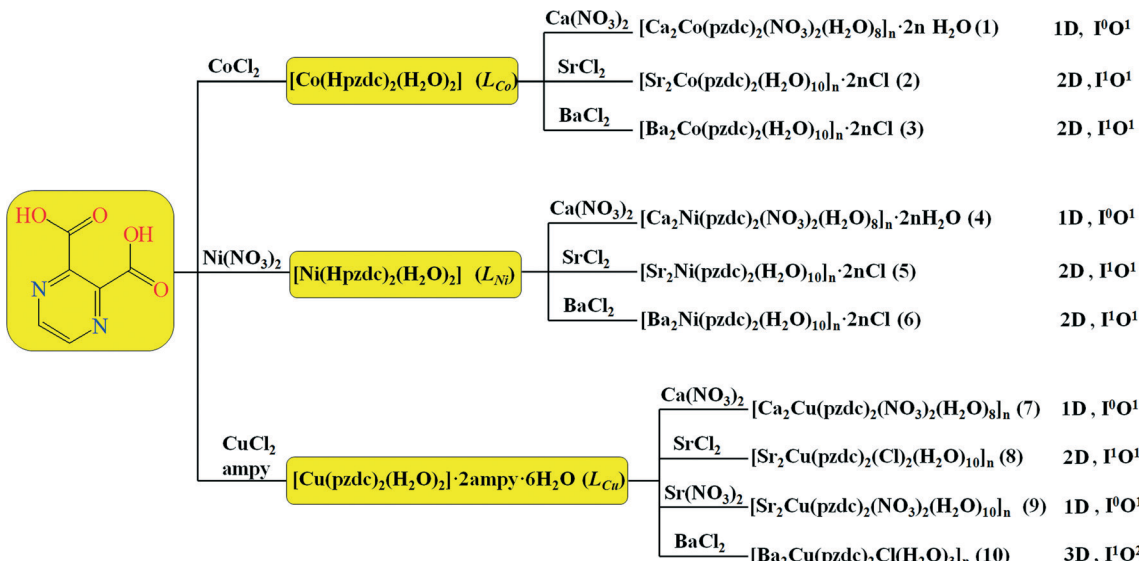
Single-crystal X-ray diffraction measurements were carried out using a Bruker SMART APEXII CCD X-ray diffractometer and a graphite crystal monochromator situated in the incident beam for data collection at 296 K. Structures were solved by direct methods and expanded with difference Fourier synthesis. Anisotropic displacement parameters were applied to all non-hydrogen atoms in full-matrix least-squares refinements based on F^2 . The H atoms were positioned geometrically and refined using a riding model with C–H = 0.097 nm, O(water)–H = 0.085 nm and with $U_{\text{iso}}(\text{H}) = 1.2U_{\text{iso}}(\text{C})$, $U_{\text{iso}}(\text{H}) = 1.5U_{\text{iso}}(\text{O})$. All calculations were performed with the SHELXTL-97 package.¹⁵ Crystallographic data for 1–10 are summarized in Table S1.† Selected bond lengths and angles of the complexes are shown in Table S2.†

Results and discussion

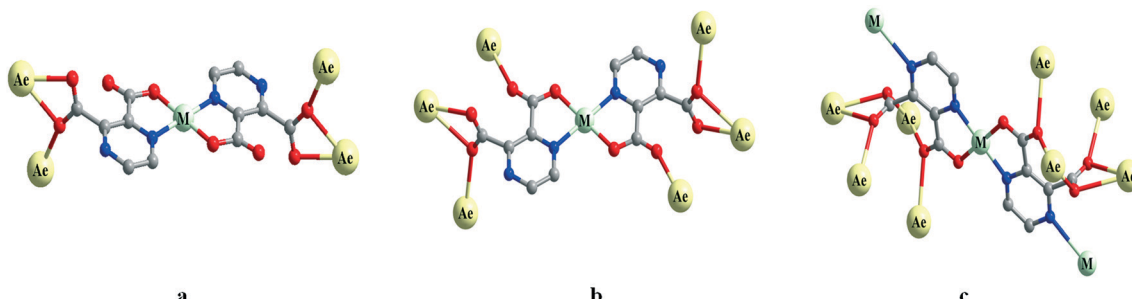
Synthesis and IR characterization

The M'MOFs were prepared through two-step reactions (Scheme 2): (1) the first step is to synthesize the precursors $[Co(Hpzdc)_2(H_2O)_2]$ (L_{Co}),^{13a} $[Ni(Hpzdc)_2(H_2O)_2]$ (L_{Ni})^{13b} and $[Cu(pzdc)_2(H_2O)_2] \cdot 2\text{ampy} \cdot 6H_2O$ (L_{Cu}),^{13c} respectively; (2) the second step is to use the precursors in reaction with the alkaline earth metal salts. The coordination environments of L_{Co} , L_{Ni} and L_{Cu} show a stable square plane $[\text{M}^{II}(pzdc)_2]^{2-}$ ($\text{M} = \text{Co}$, Ni or Cu) at the equatorial position (Fig. S1†). The bis(tetradeinate) precursors with unsaturated carboxylic oxygen atoms are inclined to coordinate with other hard metal ions (Lewis acid). Along with Ae(II) ($\text{Ae} = \text{Ca}$, Sr or Ba) added to the solution of precursors, the final mixed-metal-organic frameworks (M'MOFs) were obtained. Structural analyses illustrate that the “organic” units $[\text{M}^{II}(pzdc)_2]^{2-}$ connect with the inorganic connectivity Ae–O–Ae ($\text{Ae} = \text{Ca}$, Sr or Ba) to generate different structures from 1D to 3D with respective I^nO^m types (Schemes 2 and 3). The coordination modes of $[\text{M}^{II}(pzdc)_2]^{2-}$ units, acting as “the rigid aromatic polycarboxylate ligands”, are given as follows.

It is known that the formation of M'MOFs is strongly dependent on numerous factors including the pH value of the system, reaction temperature, reagent ratio, order of adding the starting materials, metal source and solvent.⁵ Herein, we obtained the target products at room temperature. It is found that $Ca(NO_3)_2 \cdot 4H_2O$ is a better Ca(II) source than $CaCl_2$ for the synthesis of 1, 4 and 7, while $AeCl_2$ ($\text{Ae} = \text{Sr}$ or Ba) as the Sr(II) or Ba(II) source is suitable for obtaining 2, 3, 5, 6 and 10. Interestingly, in complexes 8 and 9, we can obtain different structures using different Sr(II) sources. In a



Scheme 2 Syntheses of heteronuclear complexes 1–10.

Scheme 3 The coordination modes a–c of the plane toward metal(II) units, [M^{II}(pzdc)₂]²⁻ (M = Co, Ni or Cu), acting as a fully deprotonated ligand.

word, the anions of alkaline earth metal salts have an important role in synthesizing 1–10. The IR spectra of 1–10 are similar. The strong and broad absorption bands in the range of 3000–3500 cm⁻¹ in the spectra of complexes 1–10 are assigned as characteristic peaks of O–H vibration.¹⁶ The absence of strong absorption bands ranging from 1690 to 1730 cm⁻¹ indicates that the H₂pzdc ligand is fully deprotonated. The bands of carboxyl groups occur around 1600 cm⁻¹ for asymmetric stretching and around 1350 cm⁻¹ for symmetric stretching, in agreement with different coordination modes, such as chelating, monodentate and bridging modes. The δ_{O–C–O} vibration in plane occurs in the range of 550–860 cm⁻¹. The IR spectra of 1–10 are in accordance with the results of the X-ray diffraction analyses.¹⁷

Structural description

Crystal structures of [Ca₂Co(pzdc)₂(NO₃)₂(H₂O)₈]_n·2nH₂O (1), [Ca₂Ni(pzdc)₂(NO₃)₂(H₂O)₈]_n·2nH₂O (4) and [Ca₂Cu(pzdc)₂(NO₃)₂(H₂O)₈]_n (7). X-ray analyses performed on single crystals of complexes 1, 4 and 7 reveal an

isostructural mode possessing a 1D line structure. Hence, only the structure of 1 is described in detail. Complex 1 crystallizes in the triclinic space group *P*1, and the asymmetric unit consists of one half of a crystallographically independent Ca(II) ion, one Ca(II) ion, one pzdc²⁻ ligand, one coordinated NO₃⁻ anion, four coordinated water molecules and one free water molecule. In particular, there are no free water molecules in complex 7. As illustrated in Fig. 1a, the central Ca(II) cation is an eight-coordinated polyhedron {CaO₈} with a distorted dodecahedron geometry, including three carboxyl oxygen atoms (O₅, O_{5B} and O₆), two nitrate oxygen atoms (O₁₀ and O₂₀) and three terminal water molecules (O₁₁, O₁₃ and O₁₈). The observed bond lengths Ca–O are in the range of 2.361(4)–2.600(4) Å for 1, 2.357(4)–2.592(4) Å for 4 and 2.320(19)–2.584(2) Å for 7. The Co(II) ion displays an octahedral coordination geometry, which lies on an inversion center. The equatorial plane of Co(II) is occupied by two nitrogen atoms (Co1–N₁ = 2.103(4) Å) and two oxygen atoms (Co1–O₁ = 2.066(4) Å) from two different pzdc²⁻ ligands, displaying a [Co^{II}(pzdc)₂]²⁻ unit. The apical position is formed by two oxygen atoms (Co1–O₇ = 2.113(4) Å) from two terminal water

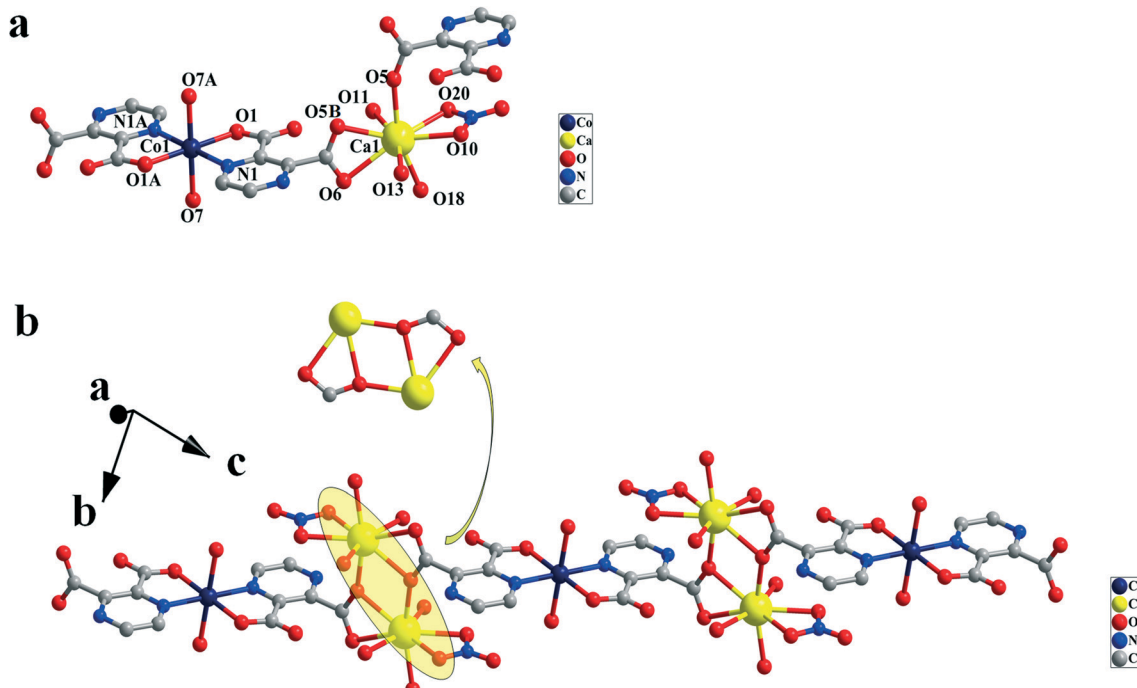


Fig. 1 (a) The coordination environments of the Co^{II} ion and the Ca^{II} ion in **1**. Symmetry codes: $A = -x + 1, -y + 1, -z$; $B = -x + 1, -y, -z + 1$. Hydrogen atoms are omitted for clarity. (b) The 1D line structure of **1** connected by the square plane $[\text{Co}^{II}(\text{pzdc})_2]^{2-}$ units and the 0D inorganic Ca–O–Ca units, classified as I⁰O¹ type.

molecules. Each $[\text{Co}^{II}(\text{pzdc})_2]^{2-}$ moiety is connected to four Ca^{II} ions through uncoordinated oxygen atoms from carboxylic groups with a $\mu_4\text{-}(\eta^2\text{-O}, \text{O}), (\eta^1\text{-O}')_2$ coordination mode (Scheme 3a). The distance of $\text{Co}^{II}\cdots\text{Co}^{II}$ is 14.459 Å. It is worth noting that two adjacent polyhedra $\{\text{CaO}_8\}_2$ are bridged by two μ_3 -carboxylate oxygen atoms to obtain a 0D Ca–O–Ca inorganic unit (Fig. 1b). The distance of $\text{Ca}^{II}\cdots\text{Ca}^{II}$ is 3.982 Å. The $[\text{Co}^{II}(\text{pzdc})_2]^{2-}$ moieties acting as “the organic ligands” link with the 0D inorganic connectivity Ca–O–Ca to obtain a 1D chain structure, classified as I⁰O¹ type (Fig. 1b).

Crystal structures of $[\text{Sr}_2\text{Co}(\text{pzdc})_2(\text{H}_2\text{O})_{10}]_n\cdot2n\text{Cl}$ (2), $[\text{Ba}_2\text{Co}(\text{pzdc})_2(\text{H}_2\text{O})_{10}]_n\cdot2n\text{Cl}$ (3), $[\text{Sr}_2\text{Ni}(\text{pzdc})_2(\text{H}_2\text{O})_{10}]_n\cdot2n\text{Cl}$ (5) and $[\text{Ba}_2\text{Ni}(\text{pzdc})_2(\text{H}_2\text{O})_{10}]_n\cdot2n\text{Cl}$ (6). X-ray structural analyses reveal that complexes 2, 3, 5, and 6 are isostructural and crystallize in the triclinic $P\bar{1}$ space group. As a representative example, the crystal structure of 2 is described in detail. The asymmetric unit of 2 contains one half of crystallographically independent Co^{II} ion, one Sr^{II} ion, one pzdc²⁻ ligand, five coordinated water molecules and one uncoordinated Cl^- anion. As shown in Fig. 2a, the Sr1 center is nine-coordinated by four carboxylic oxygen atoms (O2, O3, O4, O4C) from four pzdc²⁻ ligands and five coordinated water molecules (O6, O7, O8, O9, O8B) in a tricapped trigonal prism geometry. The bottom plane and the top plane are completed by (O4, O4C, and O9) atoms and (O2, O6, and O8) atoms, respectively, while the quadrilateral faces (O4C, O6, O8, O9), (O2, O4, O6, O9) and (O2, O4, O4C, O8) are capped by O3, O7, and O8B, respectively. The average distances of $\text{Ae}^{II}\cdots\text{O}$ are 2.664 Å for 2, 2.820 Å for 3, 2.674 Å for 5 and 2.820 Å for 6. Similar to 1,

the Co^{II} ion lies on an inversion center, displaying an octahedral coordination geometry with a $[\text{Co}(\text{pzdc})_2]^{2-}$ unit at the equatorial plane. Each $[\text{Co}^{II}(\text{pzdc})_2]^{2-}$ moiety is connected to six Sr^{II} ions through the carboxylic groups of the pzdc²⁻ ligands in a $\mu_6\text{-}(\eta^2\text{-O}, \text{O}), (\eta^1\text{-O}')_2, (\eta^1\text{-O}')$ coordination mode (Scheme 3b). Each Sr^{II} ion is connected with two neighbouring Sr^{II} ions through two $\mu_2\text{-O}$ atoms of water molecules and two μ_3 -carboxylate oxygen atoms, forming a 1D Sr–O–Sr inorganic chain (Fig. 2b). The distances of $\text{Sr}^{II}\cdots\text{Sr}^{II}$ are 4.527 Å and 4.537 Å, respectively. These Sr–O–Sr inorganic chains are connected by the $[\text{Co}(\text{pzdc})_2]^{2-}$ “organic” units to form a 2D layer structure (Fig. 2b), classified as I¹O¹ type.

Crystal structure of $[\text{Sr}_2\text{Cu}(\text{pzdc})_2(\text{Cl})_2(\text{H}_2\text{O})_{10}]_n$ (8). Single-crystal X-ray diffraction structure analysis reveals that complex 8 crystallizes in the $P\bar{1}$ space group of the triclinic system and the asymmetric unit of 8 contains one half of a Cu^{II} ion, one Sr^{II} ion, one pzdc²⁻ ligand, one coordinated Cl^- anion and five coordinated water molecules (Fig. 3a). Similar to 2, the Sr^{II} center is nine-coordinated in a tricapped trigonal prism geometry. The Cu^{II} ion lies on an inversion center, showing an octahedral geometry. Differently, the apical positions of the Cu^{II} ion are occupied by two Cl^- atoms ($\text{Cu}1\cdots\text{Cl}1 = 2.748$ (9) Å) in 8. The whole structure also shows that the Sr–O–Sr inorganic chains are connected by the $[\text{Cu}(\text{pzdc})_2]^{2-}$ “organic” connectivity to form a 2D layer structure (Fig. 3b), classified as I¹O¹ type.

Crystal structure of $[\text{Sr}_2\text{Cu}(\text{pzdc})_2(\text{NO}_3)_2(\text{H}_2\text{O})_{10}]_n$ (9). Single-crystal X-ray diffraction structure analysis reveals that complex 9 crystallizes in the $P2_1/n$ space group of the

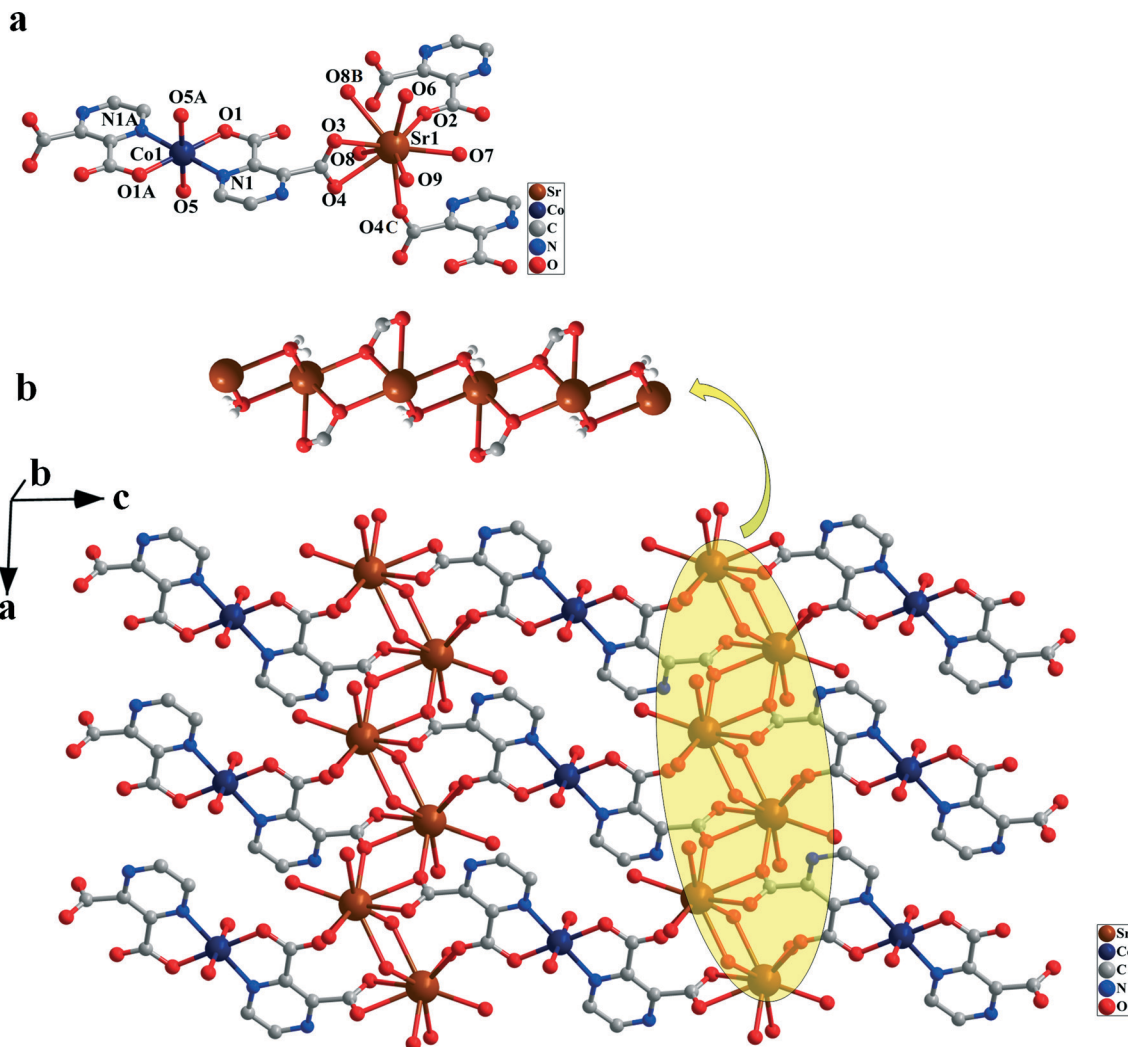


Fig. 2 (a) The coordination environments of the Co^{2+} ion and the Sr^{2+} ion in 2. Symmetry codes: $A = -x + 1, -y + 1, -z + 1; B = -x + 1, -y + 1, -z; C = x + 1, y, z$. Hydrogen atoms are omitted for clarity. (b) The 2-D layer structure of 2 connected by the square plane $[\text{Co}^{2+}(\text{pzdc})_2]^{2-}$ units and the 1D inorganic $\text{Sr}-\text{O}-\text{Sr}$ chains, classified as 1^1O^1 type.

monoclinic system. The asymmetric unit of complex 9 contains one Sr^{2+} ion, one half of a Cu^{2+} ion, one pzdc^{2-} ligand, one coordinated NO_3^- anion and five coordinated water molecules. As shown in Fig. 4a, the nine-coordinated polyhedron $\{\text{SrO}_9\}$ is constructed by three carboxylic oxygen atoms, two nitrate oxygen atoms and four aqueous oxygen atoms with a tricapped trigonal prism geometry. The $\text{Sr}-\text{O}$ lengths are in the range of $2.554(3)$ – $2.789(3)$ Å. The Cu^{2+} ion shows an octahedral geometry, which lies on an inversion center. The equatorial square is composed of two nitrogen atoms ($\text{Cu}-\text{N} = 1.987(3)$ Å) and two oxygen atoms ($\text{Cu}-\text{O} = 1.934(3)$ Å) from two different pzdc^{2-} ligands, showing a $[\text{Cu}(\text{pzdc})_2]^{2-}$ unit. The apical positions are occupied by two oxygen atoms ($\text{Cu1}-\text{O}5 = 2.550(4)$ Å) from two coordinated water molecules. Each $[\text{Cu}(\text{pzdc})_2]^{2-}$ unit adopts a $\mu_4-(\eta^2-\text{O},\text{O}),(\eta^1-\text{O}')_2$ coordination mode (Scheme 3a), coordinating with four Sr^{2+} ions. Two adjacent polyhedra $\{\text{SrO}_9\}_2$ are bridged by two μ_3 -carboxylate oxygen atoms to obtain a 0D $\text{Sr}-\text{O}-\text{Sr}$ inorganic unit (Fig. 4b).

Finally, the $[\text{Cu}(\text{pzdc})_2]^{2-}$ units connect with the adjacent $\text{Sr}-\text{O}-\text{Sr}$ inorganic units, leading to a 1D chain structure classified as 1^0O^1 type.

Crystal structure of $[\text{Ba}_2\text{Cu}(\text{pzdc})_2\text{Cl}(\text{H}_2\text{O})_5]_n$ (10). Single-crystal X-ray diffraction structure analysis reveals that complex 10 crystallizes in the monoclinic space group $C2/c$ and the asymmetric unit of 10 contains one half of a Cu^{2+} ion, one Ba^{2+} ion, one pzdc^{2-} ligand, one half of a coordinated Cl^- anion and one and a half coordinated water molecules (Fig. 5a). Cu1 lies on an inversion center, while water oxygen $\text{O}6$ and $\text{Cl}1$ lie on two-fold axes. The coordination geometry of the nine-coordinated Ba^{2+} ion is constructed by six carboxylic oxygen atoms from four different pzdc^{2-} ligands, one Cl^- anion and two oxygen atoms from two coordinated water molecules in a severely distorted monocap square anti-prismatic geometry. The $\text{Ba}-\text{O}$ lengths are in the range of $2.705(8)$ – $3.165(6)$ Å and the $\text{Ba}-\text{Cl}$ length is $3.533(8)$ Å. Each Ba^{2+} ion is bridged by three neighboring Ba^{2+} ions through

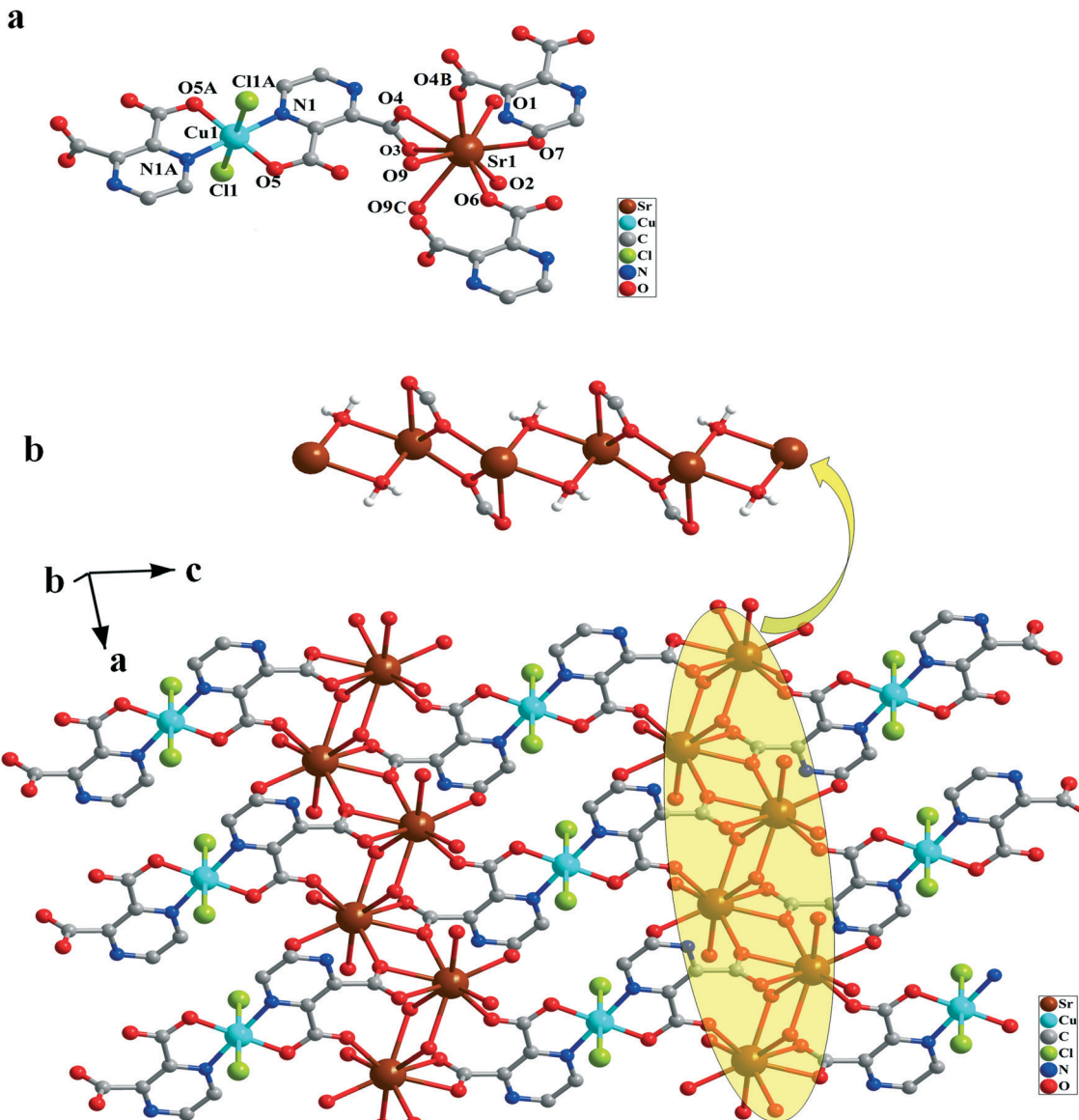


Fig. 3 (a) The coordination environments of the Cu^{II} ion and the Sr^{II} ion in **8**. Symmetry codes: A = $-x, -y + 1, -z + 2$; B = $-x + 1, -y + 1, -z + 1$; C = $-x, -y + 1, -z + 1$. Hydrogen atoms are omitted for clarity. (b) The 2-D layer structure of **8** connected by the square plane $[\text{Cu}^{\text{II}}(\text{pzdc})_2]^{2-}$ units and the 1D inorganic Sr–O–Sr chains, classified as I^1O^1 type.

one μ_2 -O atom of water molecules, one μ_2 -Cl atom and six μ_2 -carboxylate oxygen atoms to form a 1D ladder-like Ba–O–Ba inorganic chain (Fig. 5b). The distances of Ba(n)···Ba(n) are 4.530 Å, 4.571 Å and 4.861 Å, respectively. The Cu(II) ion displays an octahedral coordination geometry. The equatorial plane of Cu(II) is occupied by two nitrogen atoms (Cu–N = 2.003(9) Å) and two oxygen atoms (Cu–O = 1.942(7) Å) from two different pzdc²⁻ ligands, forming a $[\text{Cu}(\text{pzdc})_2]^{2-}$ unit. The apical position is formed by two nitrogen atoms from pyrazine rings of another two pzdc²⁻ ligands (Cu–N = 2.7123 (104) Å). These $[\text{Cu}(\text{pzdc})_2]^{2-}$ units are bridged by nitrogen atoms from pyrazine rings to generate a 2D layer structure (Fig. 5c). Finally, as shown in Fig. 5d, these layers are connected by Ba–O–Ba inorganic chains to form a 3D framework in which $[\text{Cu}(\text{pzdc})_2]^{2-}$ shows a $\mu_{10}(\eta^2-\text{O}, \text{O})_2, (\eta^1-\text{O}')$ coordination mode (Scheme 3c). The final structure can be classified as I^1O^2 type.

Discussion of the structures of 1–10

In complexes **1–10**, the bis(tetradentate) planar $[\text{M}^{\text{II}}(\text{pzdc})_2]^{2-}$ ($\text{M} = \text{Cu, Co or Ni}$) “organic” connectivity with the Ae–O–Ae (Ae = Ca, Sr, or Ba) inorganic connectivity generates different structures from 1D to 3D with three types of connectivities, the I^1O^0 connectivity for **1**, **4**, **7** and **9**, the I^1O^1 connectivity for complexes **2**, **3**, **5**, **6** and **8** and the I^1O^2 connectivity for complex **10** (Table 1). The $[\text{M}^{\text{II}}(\text{pzdc})_2]^{2-}$ moiety displays three types of coordination modes, namely $\mu_4-(\eta^2-\text{O}, \text{O})_2, (\eta^1-\text{O}')$, $\mu_6-(\eta^2-\text{O}, \text{O})_2, (\eta^1-\text{O}'), (\eta^1-\text{O}')$ and $\mu_{10}-(\eta^2-\text{O}, \text{O})_2, (\eta^2-\text{O}', \text{O}')_2, (\eta^1-\text{O}'), (\eta^1-\text{O}'), (\eta^1-\text{N}')$. In complexes **1–9**, alkaline earth metal

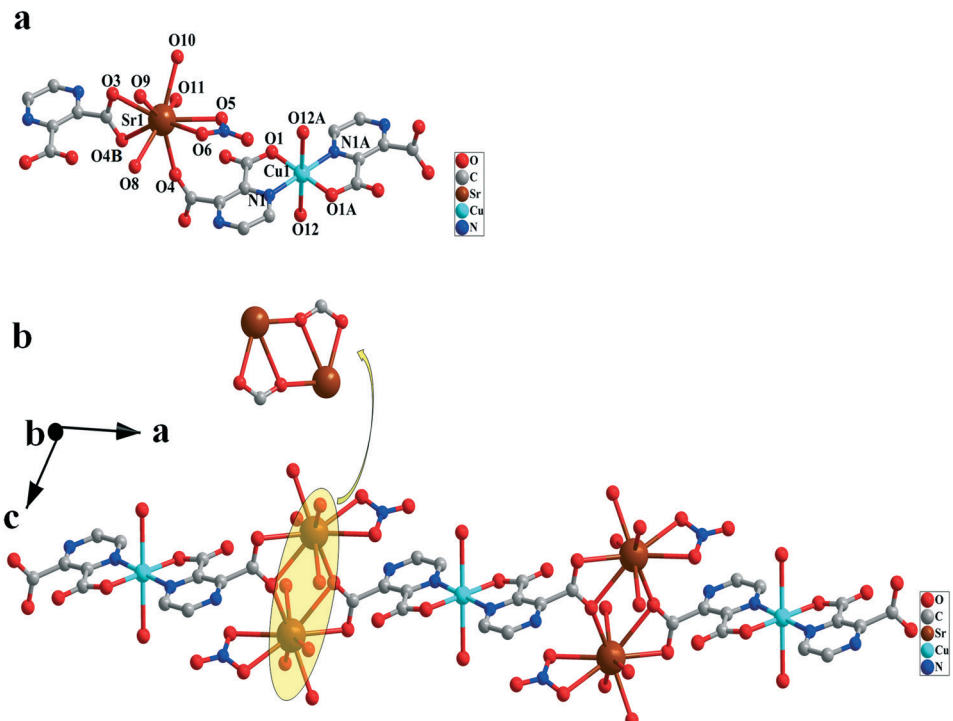


Fig. 4 (a) The coordination environments of the Cu¹ ion and the Sr¹ ion in **9**. Symmetry codes: A = -x, -y + 1, -z; B = -x + 1, -y + 1, -z. Hydrogen atoms are omitted for clarity. (b) The 2-D layer structure of **9** connected by the square plane [Cu¹¹(pzdc)₂]²⁻ units and the 1D inorganic Sr–O–Sr chains, classified as I⁰O¹ type.

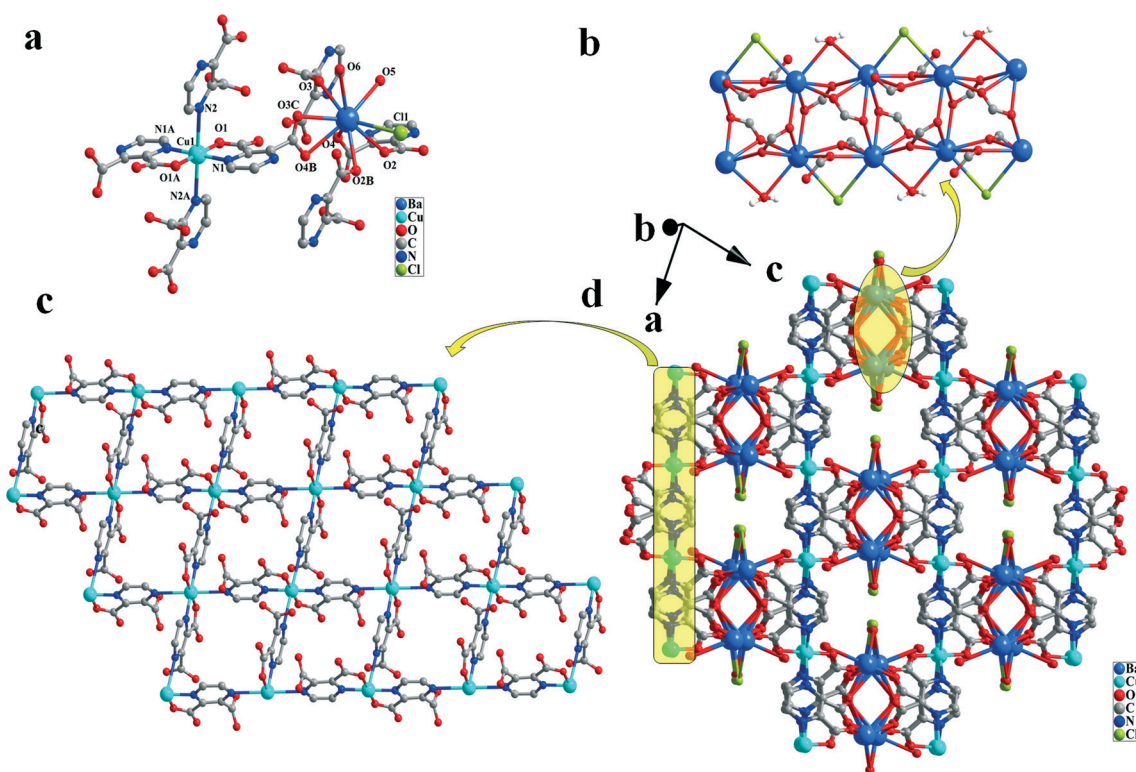


Fig. 5 (a) The coordination environments of the Cu¹ ion and the Ba¹ ion in **10**. Symmetry codes: A = -x + 3/2, -y + 3/2, -z + 1; B = -x + 1, y, -z + 1/2; C = -x + 1, -y + 1, -z + 1. Hydrogen atoms are omitted for clarity. (b) 1D inorganic Ba–O–Ba chain. (c) The [Cu(pzdc)₂]²⁻ units are bridged by nitrogen atoms from pyrazine rings to generate a 2D layer structure. (d) The 3D framework structure of **10** connected by the square planar [Cu¹¹(pzdc)₂]²⁻ units and the 1D inorganic Ba–O–Ba chains, classified as I¹O² type.

Table 1 The systematic comparisons of complexes 1–10

Complexes	$d_{\text{Ae}-\text{O}}^a$ (Å, average)	$d_{\text{M}-\text{O}}^b$ (Å)	$d_{\text{M}-\text{N}}^c$ (Å)	Dimensions of M'MOFs	Coordination modes of metalloligand unit [Cu ^{II} (pzdc) ₂] ²⁻	$d_{\text{Ae}-\text{Ae}}^d$ (Å)	$d_{\text{M}-\text{M}}^e$ (Å)	Coordination numbers and configurations	I^nO^m notion	Starting materials of Ae source
1	2.456	Plane: 2.066(4); axial: 2.113(4)	Plane: 2.103(4)	1D	Scheme 3a, μ_4 -(η^2 - O,O) ₂ ,(η^1 -O') ₂	3.982	14.459 (inter); 7.986 (intra)	8, distorted dodecahedron geometry	I^0O^1	Ca(NO ₃) ₂
2	2.664	Plane: 2.075(3); axial: 2.089(4)	Plane: 2.120(4)	2D	Scheme 3b, μ_6 -(η^2 - O,O) ₂ ,(η^1 -O') ₂ ,(η^1 - O') ₂	4.527; 4.537	13.809 (inter), 6.586 (inter); 7.642 (intra)	9, tricapped trigonal prism geometry	I^1O^1	SrCl ₂
3	2.820	Plane: 2.069(3); axial: 2.106(3)	Plane: 2.117(3)	2D	Scheme 3b, μ_6 -(η^2 - O,O) ₂ ,(η^1 -O') ₂ ,(η^1 - O') ₂	4.630; 4.780	14.094 (inter), 7.643 (inter); 6.695 (intra))	9, tricapped trigonal prism geometry	I^1O^1	BaCl ₂
4	2.448	Plane: 2.052(2); axial: 2.101(2)	Plane: 2.040(2)	1D	Scheme 3a, μ_4 -(η^2 - O,O) ₂ ,(η^1 -O') ₂	3.972	14.3563 (inter); 6.650 (intra)	8, distorted dodecahedron geometry	I^0O^1	Ca(NO ₃) ₂
5	2.674	Plane: 2.055(3); axial: 2.086(3)	Plane: 2.059(4)	2D	Scheme 3b, μ_6 -(η^2 - O,O) ₂ ,(η^1 -O') ₂ ,(η^1 - O') ₂	4.561; 4.534	13.778 (inter), 6.613 (inter); 7.651 (intra)	9, tricapped trigonal prism geometry	I^1O^1	SrCl ₂
6	2.820	Plane: 2.049(3); axial: 2.083(4)	Plane: 2.058(4)	2D	Scheme 3b, μ_6 -(η^2 - O,O) ₂ ,(η^1 -O') ₂ ,(η^1 - O') ₂	4.624; 4.787	14.034 (inter), 6.682 (inter); 7.614 (intra)	9, tricapped trigonal prism geometry	I^1O^1	BaCl ₂
7	2.458	Plane: 1.9645(18); axial: 2.538(2)	Plane: 1.990(2)	2D	Scheme 3a, μ_6 -(η^2 - O,O) ₂ ,(η^1 -O') ₂ ,(η^1 - O') ₂	3.973	14.801 (inter); 7.707 (intra)	8, distorted dodecahedron geometry	I^1O^1	Ca(NO ₃) ₂
8	2.672	Plane: 1.981(2)	Plane: 1.995(3)	2D	Scheme 3b, μ_6 -(η^2 - O,O) ₂ ,(η^1 -O') ₂ ,(η^1 - O') ₂	4.449; 4.570	13.435 (inter), 6.596 (inter); 7.787 (intra)	9, tricapped trigonal prism geometry	I^1O^1	SrCl ₂
9	2.655	Plane: 1.934(3); axial: 2.550(4)	Plane: 1.987(3)	1D	Scheme 3a, μ_4 -(η^2 - O,O) ₂ ,(η^1 -O') ₂	4.462	14.362 (inter); 6.980 (intra)	9, tricapped trigonal prism geometry	I^0O^1	Sr(NO ₃) ₂
10	2.907	Plane: 1.942(7)	Plane: 2.003(9); axial: 2.7123 (14)	3D	Scheme 3c, μ_{10} -(η^2 -O,O) ₂ ,(η^2 - O',O') ₂ ,(η^1 - O') ₂ ,(η^1 -O') ₂ ,(η^1 - N') ₂	4.530; 4.571; 4.861	7.464 (inter)	9, severely distorted monocap square antiprismatic geometry	I^1O^2	BaCl ₂

^a The average distance between alkaline earth metal cations and oxygen atoms. ^b The distances between transition metal cations and oxygen atoms (the plane sites and axial sites). ^c The distances between transition metal cations and nitrogen atoms (the plane sites and axial sites).

^d The distances of the adjacent alkaline earth metal cations. ^e The distances of the transition metal cations (in interstructure and intrastructure).

cations are surrounded by oxygen atoms from coordinated water molecules and the [M^{II}(pzdc)₂]²⁻ unit, generating polyhedra {AeO₈} or {AeO₉} in a distorted dodecahedron geometry or a tricapped trigonal prism geometry. Complex 10 shows a severely distorted monocap square antiprismatic geometry. The distances of Ae···O gradually increase from Ca to Ba, resulting from the increase in ionic radii of the group II metals.^{18,19} Complexes 2 and 3 as well as complexes 4 and 5 show different intramolecular and intermolecular distances between transition metal centers. In complexes 1–10, the different anions actually have an important role in the final structures. The presence of NO₃⁻ anion results in low-dimensional

structures, while that of Cl⁻ anion leads to high-dimensional structures. In a word, we successfully combined the strategy of “metalloligands” and the IⁿO^m notion to build transition/alkaline earth mixed-metal-organic frameworks (M'MOFs).

XRPD spectra and thermal gravimetric analysis

The phase purity of all complexes and “metalloligands” was confirmed by X-ray powder diffraction (XRPD) at room temperature (Fig. S2†). All the XRPD patterns measured for the as-synthesized samples were in good agreement with the XRPD patterns simulated from the respective single-crystal

X-ray data, indicating the phase purity of the synthesized samples. Thermogravimetric analysis (TGA) studies, performed on polycrystalline samples under oxygen-free nitrogen atmosphere with a heating rate of $10\text{ }^{\circ}\text{C min}^{-1}$ in the temperature range of $30\text{--}900\text{ }^{\circ}\text{C}$, were conducted to characterize the thermal stabilities of **1**–**10** (Fig. S3†). TG curves of **1**, **4** and **9** are very similar, showing two regions of weight losses. The first weight losses between $33\text{ }^{\circ}\text{C}$ and $125\text{ }^{\circ}\text{C}$ are 22.11% (calcd. 23.21%, **1**), 22.69% (calcd. 23.22%, **4**) and 19.26% (calcd. 20.57%, **9**), respectively, corresponding to the losses of eight coordinated water molecules and two free water molecules. The second weight losses above $250\text{ }^{\circ}\text{C}$ stem from the decomposition of the whole framework of **1**, **4** and **9**. In **7**, the coordinated water molecules escape from the framework over the range of $110\text{--}160\text{ }^{\circ}\text{C}$ with an observed weight loss of 18.29% (calcd. 19.35%). Then the dehydrated sample can be stable up to $250\text{ }^{\circ}\text{C}$. Upon heating, the framework begins to collapse owing to the decomposition of the pzdc²⁻ ligands and NO₃⁻ anions. Complexes **2**, **3**, **5** and **6** possess two obvious steps of weight losses. The first weight losses that occur in the range $100\text{--}130\text{ }^{\circ}\text{C}$ are 29.11% (calcd. 30.71%, **2**), 28.01% (calcd. 27.38%, **3**), 29.22% (calcd. 30.71%, **5**) and 29.01% (calcd. 27.38%, **6**), respectively, which agree with the losses of all coordinated water molecules. Above $345\text{ }^{\circ}\text{C}$, the frameworks begin to collapse and gradually decompose to complicated oxides. For **8**, there is a weight loss of 22.11% in the temperature range of $116\text{--}168\text{ }^{\circ}\text{C}$, corresponding to the release of the coordinated water molecules (calcd. 21.90%). Then a continuous weight loss indicates the decomposition of the whole framework. For **10**, the release of three coordinated water molecules per formula unit occurs in the range of $140\text{--}160\text{ }^{\circ}\text{C}$ and the observed weight loss of 6.77% is in agreement with the calculated value (7.10%). The dehydrated sample can be stable up to $450\text{ }^{\circ}\text{C}$, followed by a slow collapse of the framework.

Magnetic properties

Magnetic properties of **1 and **2**.** Variable-temperature dc magnetic susceptibility data were recorded for polycrystalline samples of **1** and **2** in the temperature range of $2\text{--}300\text{ K}$. The $\chi_M T$ values of **1** and **2** at 300 K are $2.87\text{ cm}^3\text{ K mol}^{-1}$ and $2.57\text{ cm}^3\text{ K mol}^{-1}$ (Fig. 6 and 7), respectively, which exceed the spin-only value for one isolated Co(II) ion ($1.875\text{ cm}^3\text{ K mol}^{-1}$, $S = 3/2$ and $g = 2.0$).^{20–22} This is indicative of an unquenched orbital contribution of the Co(II) ion in a distorted octahedral geometry. The $\chi_M T$ values of **1** and **2** gradually decrease to $2.41\text{ cm}^3\text{ K mol}^{-1}$ at 50 K and $2.19\text{ cm}^3\text{ K mol}^{-1}$ at 60 K and then at lower temperatures decrease more steeply to reach $1.69\text{ cm}^3\text{ K mol}^{-1}$ and $1.83\text{ cm}^3\text{ K mol}^{-1}$ at 2 K , respectively. As the neighboring Co(II) ions are separated by Ca(II) or Sr(II) ions, with Co(II)–Co(II) distances being longer than 13.000 \AA , it is proposed that the orbital momentum contributes to the decrease in magnetic susceptibility with decreasing temperature.^{5b,23} The plots of χ_M^{-1} versus T of **1** and **2** over the temperature range from 50 K to 300 K and 60 K to 300 K

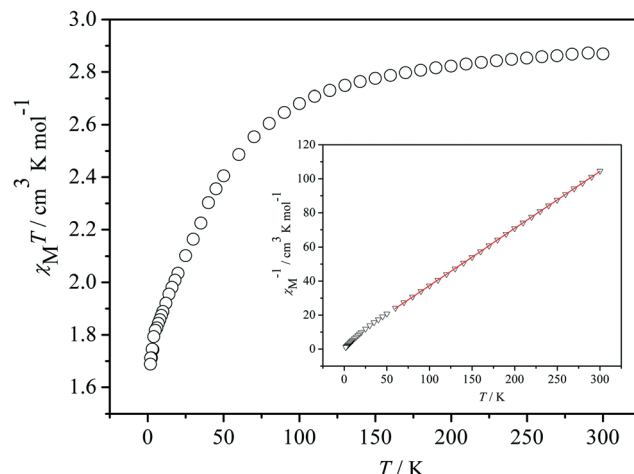


Fig. 6 Temperature dependence of magnetic susceptibilities in the form of $\chi_M T$ versus T for **1**. Inset: temperature dependence of magnetic susceptibilities in the form of χ_M^{-1} versus T . The solid line corresponds to the best fit from 300 K to 50 K .

obey the Curie–Weiss law [$\chi = C/(T - \theta)$] with $C = 2.984\text{ cm}^3\text{ K mol}^{-1}$ and $\theta = -11.44\text{ K}$ as well as $C = 2.689\text{ cm}^3\text{ K mol}^{-1}$ and $\theta = -13.277\text{ K}$, respectively. The decrease in $\chi_M T$ curves with a decrease in temperature and the negative values of θ indicate the contribution of spin-orbital coupling of the single Co(II) ion. The values of the magnetisation *vs.* H plot for **1** and **2** at 2.0 K led to quasi-saturation values of $2.08\text{ N}\beta$ and $2.06\text{ N}\beta$ at 5 T (Fig. S4 and S5†), respectively. The values are as expected for one six-coordinate high-spin Co(II) ion.

Magnetic properties of **4 and **5**.** The room temperature $\chi_M T$ value for **4** is $1.26\text{ cm}^3\text{ K mol}^{-1}$ (Fig. 8), which is close to the expected value of $1.00\text{ cm}^3\text{ K mol}^{-1}$ for one $S = 1$ spin for the Ni(II) ion with $g = 2$.^{5,24} The $\chi_M T$ values decrease slightly with decreasing temperature from 300 K to 31 K and then decrease more rapidly to a value of $0.876\text{ cm}^3\text{ K mol}^{-1}$ at 2 K . The interactions of the Ni(II) ions in the range of $2\text{--}300\text{ K}$ are

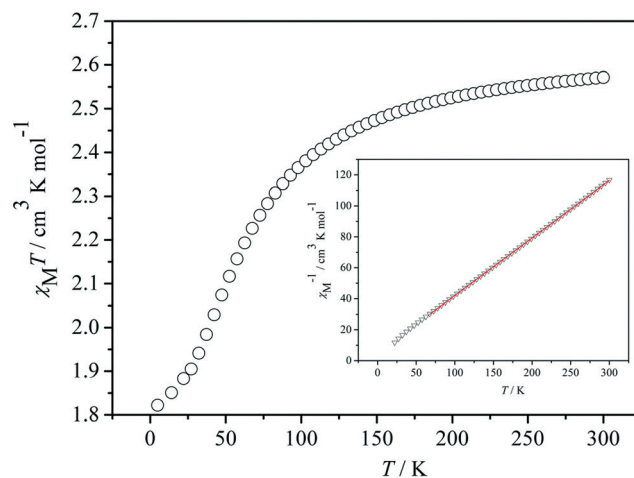


Fig. 7 Temperature dependence of magnetic susceptibilities in the form of $\chi_M T$ versus T for **2**. Inset: temperature dependence of magnetic susceptibilities in the form of χ_M^{-1} versus T . The solid line corresponds to the best fit from 300 K to 60 K .

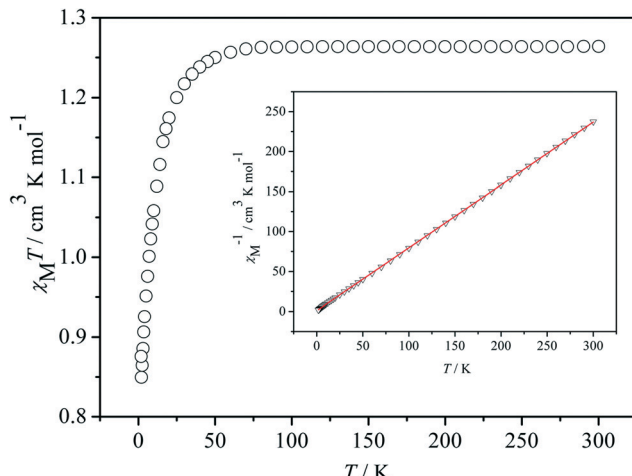


Fig. 8 Temperature dependence of magnetic susceptibilities in the form of $\chi_M T$ versus T for **4**. Inset: temperature dependence of magnetic susceptibilities in the form of χ_M^{-1} versus T . The solid line corresponds to the best fit from 300 K to 2 K.

fitted using the Curie–Weiss law, $1/\chi_M = (T - \theta)/C$, with Curie constant $C = 1.272 \text{ cm}^3 \text{ K mol}^{-1}$ and Weiss constant $\theta = -1.325 \text{ K}$. As shown in Fig. 9, the $\chi_M T$ value is $1.71 \text{ cm}^3 \text{ K mol}^{-1}$ at 300 K, which is larger than the spin-only value ($1.0 \text{ cm}^3 \text{ K mol}^{-1}$) for an isolated Ni(II) cation ($S = 1$). As the temperature decreases, the $\chi_M T$ values gradually decrease. However, the pronounced decreases are observed until below 50 K and the minimal value is observed at 2 K. The parameters fitted using the Curie–Weiss law above 30 K are obtained to be $C = 1.811 \text{ cm}^3 \text{ K mol}^{-1}$ and $\theta = -8.601 \text{ K}$. From the structural perspective, the neighboring Ni(II) ions are well separated by Ca(II) or Sr(II) ions with $\text{Ni(II)} \cdots \text{Ni(II)}$ distances being longer than 13.000 \AA . So in compounds **4** and **5**, the decrease in $\chi_M T$ curves with a decrease in temperature may

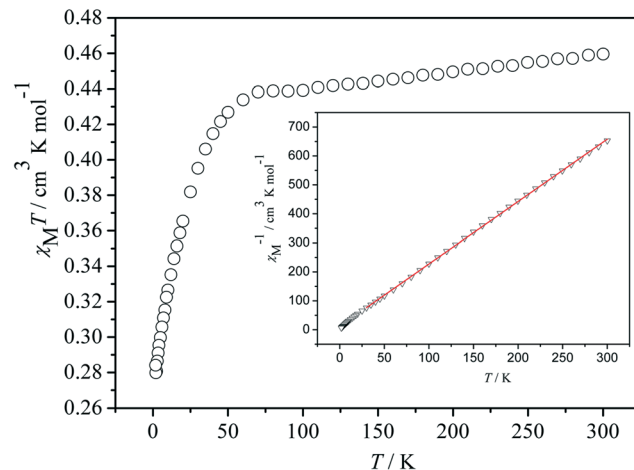


Fig. 10 Temperature dependence of magnetic susceptibilities in the form of $\chi_M T$ versus T for **10**. Inset: temperature dependence of magnetic susceptibilities in the form of χ_M^{-1} versus T . The solid line corresponds to the best fit from 300 K to 25 K.

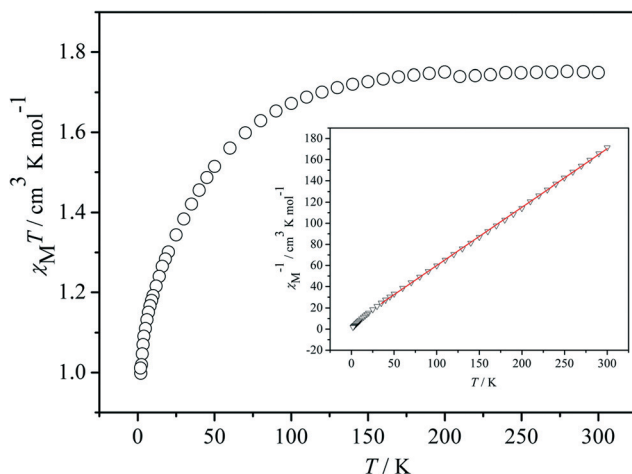


Fig. 9 Temperature dependence of magnetic susceptibilities in the form of $\chi_M T$ versus T for **5**. Inset: temperature dependence of magnetic susceptibilities in the form of χ_M^{-1} versus T . The solid line corresponds to the best fit from 300 K to 30 K.

be caused by the single-ion anisotropy of Ni(II) ions. The values of the magnetisation vs. H plot for **4** and **5** at 2.0 K lead to values of $1.83 \text{ N}\beta$ and $1.92 \text{ N}\beta$ at 5 T (Fig. S6 and S7†), respectively. The values are as expected for one single-ion anisotropy of Ni(II) ions.

Magnetic properties of 10. Magnetic susceptibility data of **10** are obtained in the range of 2–300 K (Fig. 10). As can be seen, the $\chi_M T$ product for **10** at room temperature is $0.460 \text{ cm}^3 \text{ K mol}^{-1}$, which is larger than the expected value of $0.375 \text{ cm}^3 \text{ K mol}^{-1}$ for one $S = 1/2$ uncoupled spin. The $\chi_M T$ product decreases steadily with decreasing temperature in the range of 300–25 K, before decreasing more rapidly below this temperature to a value of $0.284 \text{ cm}^3 \text{ K mol}^{-1}$ at 1.9 K. This behavior is indicative of the presence of antiferromagnetic exchange interactions between the metal ions through pyrazine rings of pzdc^{2-} .²⁵ Several magnetic studies of polynuclear copper complexes bridged by pyz (pyrazine) have been reported, such as $\text{Cu}(\text{pyz})(\text{NO}_3)_2$ (ref. 26) and $\text{Cu}(\text{pyz})(\text{CF}_3\text{SO}_3)_2$ (ref. 27), showing antiferromagnetic exchange interactions. The plots of χ_M^{-1} versus T over the temperature range from 25 K to 300 K obey the Curie–Weiss law [$\chi = C/(T - \theta)$] with $C = 0.464 \text{ cm}^3 \text{ K mol}^{-1}$ and $\theta = -5.488 \text{ K}$. The increase in $\chi_M T$ and the negative value of θ indicate the existence of antiferromagnetic interactions. At 2 K, the field-dependent magnetization increases linearly to a maximum value of $0.75 \text{ N}\beta$ (Fig. S8†), indicating that the magnetic moment is still unsaturated (the expected saturated value is $M_s = nSg = 1 \text{ N}\beta$). This behaviour is probably due to the significant antiferromagnetic interactions between the Cu(II) ions since the Cu(II) ions are not so anisotropic.

Conclusions

Ten new mixed-metal–organic frameworks (M'MOFs) with alkaline-earth metal ions and transition metal ions were controllably synthesized through the reaction of bis(tetrade-

“metalloligands” with different alkaline earth metal salts at room temperature. In complexes **1–10**, the bis(tetradeinate) $[M^{II}(pzdc)_2]^{2-}$ ($M = Cu, Co$ or Ni) “organic” connectivity and the $Ae-O-Ae$ ($Ae = Ca, Sr$, or Ba) inorganic connectivity generate different structures from 1D to 3D with three types of connectivities, the I^1O^0 connectivity for **1**, **4**, **7** and **9**, the I^1O^1 connectivity for complexes **2**, **3**, **5**, **6** and **8** and the I^1O^2 connectivity for complex **10**. The ionic radii of cations and the different anions of alkaline-earth metal salts have an important influence on the structural diversities. As the neighboring M^{II} ions ($M = Co$ or Ni) are separated by Ae^{II} ions ($Ae = Ca$ or Sr), with $M^{II}\cdots M^{II}$ distances being longer than 13.000 Å, it is proposed that the decrease in χ_{MT} curves with decreasing temperature of compounds **1** and **2** as well as compounds **4** and **5** should be caused by the behavior of single Co^{II} ions and the single-ion anisotropy of Ni^{II} ions, respectively. The magnetic studies of **10** reveal the existence of antiferromagnetic interactions between the metal ions through pyrazine rings of $pzdc^{2-}$.

Based on the I^nO^m notion, a controllable “metalloligand” strategy is feasible to obtain $M' MOFs$. Moreover, these results would be helpful in synthesizing new $M' MOFs$ with intriguing structures as well as outstanding properties from a new perspective of crystallographic engineering.

Acknowledgements

We gratefully acknowledge financial support from the National Natural Science Foundation of China (grant no. 21373162, 21463020, 21073142 and 21173168), the Natural Science Foundation of Shanxi Province (grant no. 11JS110, 2013JM2002 and SJ08B09), and the Postgraduate Innovation Foundation of Northwest University (YZZ13046).

References

- 1 K. M. Fromm, *Coord. Chem. Rev.*, 2008, **252**, 856.
- 2 (a) S. Harder, *Angew. Chem., Int. Ed.*, 2003, **42**, 3430; (b) X. Lin, D. M. Doble, A. J. Blake, A. Harrison, C. Wilson and M. Schroder, *J. Am. Chem. Soc.*, 2003, **125**, 9476.
- 3 (a) R. Cao, J. Lü and S. R. Batten, *CrystEngComm*, 2008, **10**, 784; (b) Y. Zhang, X. B. Luo, Z. L. Yang and G. Li, *CrystEngComm*, 2012, **14**, 7382.
- 4 (a) X. Zhang, Y. Y. Huang, J. K. Cheng, Y. G. Yao, J. Zhang and F. Wang, *CrystEngComm*, 2012, **14**, 4843; (b) S. Akine, T. Tadokoro and T. Nabeshima, *Inorg. Chem.*, 2012, **51**, 11478; (c) M. Insausti, J. L. Pizarro, L. Lezama, R. Cortes, E. H. Bocanegra, M. I. Arriortua and T. Rojo, *Chem. Mater.*, 1994, **6**, 707; (d) I. Gil de Muro, F. A. Mautner, M. Insausti, L. Lezama, M. I. Arriortua and T. Rojo, *Inorg. Chem.*, 1998, **37**, 3243; (e) G. Aromi, O. Roubeau, M. Helliwell, S. J. Teat and R. E. P. Winpenny, *Dalton Trans.*, 2003, 3436; (f) D. Prodius, C. Turta, V. Mereacre, S. Shova, M. Gdaniec, Y. Simonov, J. Lipkowski, V. Kunser, G. Filoti and A. Caneschi, *Polyhedron*, 2006, **25**, 2175; (g) G. E. Kostakis, A. M. Ako and A. K. Powell, *Chem. Soc. Rev.*, 2010, **39**, 2238; (h) G. B. Deacon, P. C. Junk, G. J. Moxey, K. Ruhlandt-Senge, C. St Prix and M. F. Zuniga, *Chem. – Eur. J.*, 2009, **15**, 5503; (i) T. K. Prasad and M. V. Rajasekharan, *Inorg. Chem. Commun.*, 2005, **8**, 1116; (j) A. Lazarescu, S. Shova, J. Bartolome, P. Alonso, A. Arauzo, A. M. Balu, Y. A. Simonov, M. Gdaniec, C. Turta, G. Filoti and R. Luque, *Dalton Trans.*, 2011, **40**, 463.
- 5 (a) Y. M. Chen, S. X. She, Q. Gao, D. D. Gao, D. R. Wang, Y. H. Li, W. Liu and W. Li, *CrystEngComm*, 2014, **16**, 1091; (b) Y. M. Chen, Q. Gao, H. F. Zhang, D. D. Gao, Y. H. Li, W. Liu and W. Li, *Polyhedron*, 2014, **71**, 91; (c) Y. M. Chen, Q. Gao, W. Q. Chen, D. D. Gao, Y. H. Li, W. Liu and W. Li, *Chem. – Asian J.*, 2015, **12**, 411; (d) Y. M. Chen, L. N. Zheng, S. X. She, Z. Chen, B. Hu and Y. H. Li, *Dalton Trans.*, 2011, **40**, 4970.
- 6 (a) E. Pardo, R. Ruiz-García, F. Lloret, J. Faus, M. Julve, Y. Journaux, M. A. Novak, F. S. Delgado and C. Ruiz-Pérez, *Chem. – Eur. J.*, 2007, **13**, 2054; (b) J. Ferrando-Soria, E. Pardo, R. Ruiz-García, J. Cano, F. Lloret, M. Julve, Y. Journaux, J. Pasán and C. Ruiz-Pérez, *Chem. – Eur. J.*, 2011, **17**, 2176.
- 7 (a) S. J. Garibay, J. R. Stork and S. M. Cohen, *Prog. Inorg. Chem.*, 2009, **56**, 335; (b) B. Chen, S. Xiang and G. Qian, *Acc. Chem. Res.*, 2010, **43**, 1115; (c) O. Kahn, *Acc. Chem. Res.*, 2000, **33**, 647; (d) B. Q. Ma, S. Gao, G. Su and G. X. Xu, *Angew. Chem., Int. Ed.*, 2001, **40**, 434; (e) H. Fenton, I. S. Tidmarsh and M. D. Ward, *Dalton Trans.*, 2010, **39**, 3805.
- 8 (a) M. C. Das, S. C. Xiang, Z. J. Zhang and B. L. Chen, *Angew. Chem., Int. Ed.*, 2011, **50**, 10510; (b) H. B. Wu and Q. M. Wang, *Angew. Chem., Int. Ed.*, 2009, **48**, 7343; (c) V. D. Vreshch, A. B. Lysenko, A. N. Chernega, J. A. K. Howard, H. Krautscheid, J. Sielerd and K. V. Domasevitch, *Dalton Trans.*, 2004, 2899; (d) J. H. Zhang, S. M. Cheng, X. F. Wang, L. M. Yuan, M. Q. Xue, Y. Wang and W. L. Liu, *CrystEngComm*, 2013, **15**, 6074; (e) D. M. Ciurtin, M. D. Smith and H.-C. zur Loye, *Inorg. Chim. Acta*, 2001, **324**, 46.
- 9 L. Zhang, Z. J. Li, Q. P. Lin, Y. Y. Qin, J. Zhang, P. X. Yin, J. K. Cheng and Y. G. Yao, *Inorg. Chem.*, 2009, **48**, 6517.
- 10 (a) A. K. Cheetham and C. N. R. Rao, *Science*, 2007, **318**, 58; (b) C. N. R. Rao, A. K. Cheetham and A. Thirumurugan, *J. Phys.: Condens. Matter*, 2008, **20**, 083202.
- 11 (a) S. Kitagawa and K. Uemura, *Chem. Soc. Rev.*, 2005, **34**, 109; (b) D. S. Li, Y. P. Wu, J. Zhao, J. Zhang and J. Y. Luc, *Chem. Soc. Rev.*, 2014, **261**, 1; (c) W. G. Lu, Z. W. Wei, Z. Y. Gu, T. F. Liu, J. H. Park, J. Park, J. Tian, M. W. Zhang, Q. Zhang, T. Gentle III, M. Boscha and H. C. Zhou, *Chem. Soc. Rev.*, 2014, **43**, 5561; (d) Y. Z. Zheng, Z. P. Zheng and X. M. Chen, *Chem. Soc. Rev.*, 2014, **258**, 1; (e) J. W. Liu, L. F. Chen, H. Cui, J. Y. Zhang, L. Zhang and C. Y. Su, *Chem. Soc. Rev.*, 2014, **43**, 6011; (f) Z. J. Lin and M. L. Tong, *Coord. Chem. Rev.*, 2011, **255**, 421; (g) M. Du, M. Chen, X. G. Yang, J. Wen, X. Wang, S. M. Fang and C. S. Liu, *J. Mater. Chem. A*, 2014, **2**, 9828; (h) X. H. Chang, Y. Zhao, M. L. Han, L. F. Ma and L. Y. Wang, *CrystEngComm*, 2014, **16**, 6417; (i) M. L. Han, X. H. Chang, X. Feng, L. F. Ma and L. Y. Wang, *CrystEngComm*, 2014, **16**, 1687; (j) Y. Q. Xu, D. Q. Yuan, B. L. Wu, L. Han, M. Y. Wu, F. L. Jiang and M. C. Hong,

- Cryst. Growth Des.*, 2006, **6**, 1168; (k) Y. L. Gai, F. L. Jiang, L. Chen, M. Y. Wu, K. Z. Su, J. Pan, X. Y. Wan and M. C. Hong, *Cryst. Growth Des.*, 2014, **14**, 1010.
- 12 X. Zhang, Y. Y. Huang, M. J. Zhang, J. Zhang and Y. G. Yao, *Cryst. Growth Des.*, 2012, **12**, 3231.
- 13 (a) C. J. O'Connor and E. Sinn, *Inorg. Chem.*, 1981, **20**, 545. Synthesis of $[\text{Co}(\text{Hpzdc})_2(\text{H}_2\text{O})_2]$ (L_{Co}): a 5 mmol sample of pyrazine-carboxylate was dissolved in 150 mL of H_2O . A 2.5 mmol sample of cobalt(II) chloride was dissolved in 25 mL of H_2O . The solutions were mixed, and single crystals suitable for X-ray analysis were obtained after the solutions were left to stand overnight. This was confirmed by PXRD (Fig. S2a, see the ESI). Anal. calcd. for $\text{C}_{12}\text{H}_{10}\text{CoN}_4\text{O}_{10}$ (429.17): C 33.55%, H 2.33%, N 13.05%; found: C 33.43%, H 2.22%, N 13.16%. IR data (KBr pellet): 3233(m), 1638(s), 1590(m), 1557(m), 1355(s), 1323(s), 1146(s), 1133(m), 1058(s), 832(m), 811(s), 701(m), 612(m), 532(m), 467(m), 410(s); (b) L. Mao, S. J. Rettig, R. C. Thompson, J. Trotter and S. H. Xia, *Can. J. Chem.*, 1996, **74**, 433. Synthesis of $[\text{Ni}(\text{Hpzdc})_2(\text{H}_2\text{O})_2]$ (L_{Ni}): 2,3-pyrazinedicarboxylic acid (0.42 g, 2.5 mmol) was dissolved in 60 mL of water and slowly added to a 60 mL aqueous solution of $\text{Ni}(\text{NO}_3)_2 \cdot 6\text{H}_2\text{O}$ (0.36 g, 1.25 mmol). After the solution was left to stand for 2–3 weeks, green crystals were obtained. This was confirmed by PXRD (Fig. S2b, see the ESI). Anal. calcd. for $\text{C}_{12}\text{H}_{10}\text{N}_4\text{NiO}_{10}$ (428.93): C 33.60%, H 2.35%, N 13.06%; found: C 33.79%, H 2.51%, N 13.11%. IR data (KBr pellet): 3250(m), 1656(s), 1590(m), 1578(m), 1344(s), 1334(s), 1167(s), 1145(m), 1050(s), 834(m), 789(s), 722(m), 633(s), 561(s), 510(m), 432(s); (c) H. Eshtiagh-Hosseini, F. Gschwind, N. Alfi and M. Mirzaei, *Acta Crystallogr., Sect. E: Struct. Rep. Online*, 2010, **66**, m826. Synthesis of $[\text{Cu}(\text{pzdc})_2(\text{H}_2\text{O})_2] \cdot 2\text{ampy} \cdot 6\text{H}_2\text{O}$ (L_{Cu}): a solution of H_2pzdc (0.18 mmol, 0.03 mg) in water (10 ml) was refluxed for 1 hour, then a solution of $\text{CuCl}_2 \cdot 6\text{H}_2\text{O}$ (0.02 mmol, 0.01 g) was added dropwise, followed by 1 mmol of 2-amino-4-methylpyridine (99%, ampy) and the solution was continuously refluxed for 6 hours at 60 °C. The obtained blue solution gave blue block-like crystals of the title complex after slow evaporation of solvent at room temperature. This was confirmed by PXRD (Fig. S2c, see the ESI). Anal. calcd for $\text{C}_{24}\text{H}_{38}\text{CuN}_8\text{O}_{16}$ (758.17): C 37.99%, H 5.01%, N 14.77%; found: C 38.05%, H 5.11%, N 14.58%. IR data (KBr pellet): 3255(br), 1655(s), 1644(s), 1587(m), 1544(m), 1365(s), 1311(s), 1159(s), 1155(m), 1045(s), 811(m), 803(s), 710(m), 649(m), 550(m), 499(m), 418(s).
- 14 (a) Y. Kubota, M. Takata, R. Matsuda, R. Kitaura, S. Kitagawa and T. C. Kobayashi, *Angew. Chem., Int. Ed.*, 2004, **43**, 2334; (b) D. Xie, J. Ye and Z. Liu, *Inorg. Chem. Commun.*, 2009, **12**, 72; (c) Z. L. Xu, X. Y. Li and G. B. Che, *Chin. J. Struct. Chem.*, 2008, **27**, 593; (d) Y. L. Niu, X. M. Li and B. Liu, *Chin. J. Struct. Chem.*, 2010, **29**, 712; (e) E. H. Hossein, H. Azam and A. Nafiseh, *J. Coord. Chem.*, 2010, **63**, 3175; (f) T. L. Che, Q. C. Gao, W. P. Zhang, Z. X. Nan, H. X. Li, Y. G. Cai and J. S. Zhao, *Russ. J. Coord. Chem.*, 2009, **35**, 723; (g) S. Zhang, Q. Wei, G. Xie, Q. Yang and S. P. Chen, *Inorg. Chim. Acta*, 2012, **387**, 52; (h) Q. Yang, G. Xie, Q. Wei, S. P. Chen and S. L. Gao, *J. Solid State Chem.*, 2014, **215**, 26; (i) S. Zhang, X. N. Qu, G. Xie, Q. Wei and S. P. Chen, *J. Solid State Chem.*, 2013, **210**, 36.
- 15 (a) G. M. Sheldrick, *SHELXS-97, Program for Solution of Crystal Structures*, University of Göttingen, Germany, 1997; (b) G. M. Sheldrick, *SHELXL-97, Program for Refinement of Crystal Structures*, University of Göttingen, Germany, 1997.
- 16 (a) I. Sakiyan, *Transition Met. Chem.*, 2007, **32**, 131; (b) M. Shebl, *Spectrochim. Acta, Part A*, 2009, **73**, 313.
- 17 (a) Y. Thio, S. Wei Toh, F. Xue and J. J. Vittal, *Dalton Trans.*, 2014, **43**, 5998; (b) M. S. Shongwe, M. Mikuriya, R. Nukada, E. W. Ainscough, A. M. Brodie and J. M. Waters, *Inorg. Chim. Acta*, 1999, **290**, 228; (c) G. B. Deacon and R. J. Phillip, *Coord. Chem. Rev.*, 1980, **33**, 227; (d) J. Xu, J. W. Cheng, W. P. Su and M. C. Hong, *Cryst. Growth Des.*, 2011, **11**, 2294.
- 18 C. A. Williams, A. J. Blake, C. Wilson, P. Hubberstey and M. Schröder, *Cryst. Growth Des.*, 2008, **8**, 911.
- 19 J. Emsley, *The Elements*, Oxford University Guides, 2nd edn, 1991.
- 20 V. Chandrasekhar, A. Dey, A. J. Mota and E. Colacio, *Inorg. Chem.*, 2013, **52**, 4554.
- 21 (a) M. Murrie, *Chem. Soc. Rev.*, 2010, **39**, 1986; (b) F. Lloret, M. Julve, J. Cano, R. Ruiz-Garcia and E. Pardo, *Inorg. Chim. Acta*, 2008, **361**, 3432; (c) O. Kahn, *Molecular Magnetism*, VCH Publishers Inc, New York, 1993; (d) M. Lamouchi, E. Jeanneau, G. Novitchi, D. Luneau, A. Brioude and C. Desroches, *Inorg. Chem.*, 2014, **53**, 63; (e) J. Vallejo, I. Castro, R. Ruiz-García, J. Cano, M. Julve, F. Lloret, G. D. Munno, W. Wernsdorfer and E. Pardo, *J. Am. Chem. Soc.*, 2012, **134**, 15704; (f) D. S. Li, J. Zhao, Y. P. Wu, B. Liu, L. Bai, K. Zou and M. Du, *Inorg. Chem.*, 2013, **52**, 8091.
- 22 S. Konar, P. S. Mukherjee, M. G. B. Drew, J. Ribas and N. R. Chaudhuri, *Inorg. Chem.*, 2003, **42**, 2545.
- 23 X. X. Hu, J. Q. Xu, P. Cheng, X. Y. Chen, X. B. Cui, J. F. Song, G. D. Yang and T. G. Wang, *Inorg. Chem.*, 2004, **43**, 2261.
- 24 G. Marinescu, M. Andruh, M. Julve, F. Lloret, R. Llusar, S. Uriel and J. Vaissermann, *Cryst. Growth Des.*, 2005, **5**, 261.
- 25 T. Okubo, M. Kondo and S. Kitagawa, *Synth. Met.*, 1997, **85**, 1661.
- 26 P. D. Boyd and S. Mitra, *Inorg. Chem.*, 1980, **19**, 3547.
- 27 J. S. Haynes, S. J. Rettig, J. R. Sams, J. Trotter and R. C. Thompson, *Inorg. Chem.*, 1988, **27**, 1237.